Hindawi Publishing Corporation
Journal of Nanomaterials
Volume 2011, Article ID 753705, 8 pages
doi:10.1155/2011/753705

Research Article

Preparation of Rhodamine B Fluorescent Poly(methacrylic acid) Coated Gelatin Nanoparticles

Zhenhai Gan,[1] Jianhui Ju,[1] Ting Zhang,[2] and Daocheng Wu[1]

[1] *Key Laboratory of Biomedical Information Engineering of Education Ministry, School of Life Science and Technology, Xi'an Jiaotong University, Xi'an 710049, China*
[2] *Scientific Research Center, The Second Affiliated Hospital, School of Medicine, Xi'an Jiaotong University, Xi'an 710004, China*

Correspondence should be addressed to Daocheng Wu, wudaocheng@mail.xjtu.edu.cn

Received 29 April 2011; Revised 24 June 2011; Accepted 26 June 2011

Academic Editor: Xing J. Liang

Poly(methacrylic acid) (PMAA)-coated gelatin nanoparticles encapsulated with fluorescent dye rhodamine B were prepared by the coacervation method with the aim to retard the release of rhodamine B from the gelatin matrix. With sodium sulfate as coacervation reagent for gelatin, a kind of biopolymer with excellent biocompatibility, the formed gelatin nanoparticles were cross-linked by formaldehyde followed by the polymerization of methacrylic acid coating. The fluorescent poly(methacrylic acid) coated gelatin (FPMAAG) nanoparticles had a uniform spherical shape and a size distribution of 60 ± 5 nm. Infrared spectral analysis confirmed the formation of PMAA coating on the gelatin nanoparticles. Based on UV-Vis spectra, the loading efficiency of rhodamine B for the FPMAAG nanoparticles was 0.26 μg per mg nanoparticles. The encapsulated rhodamine B could sustain for two weeks. Favorable fluorescence property and fluorescence imaging of cells confirmed that the FPMAAG nanoparticles have promising biochemical, bioanalytical, and biomedical applications.

1. Introduction

Recently, various kinds of functional nanoparticles have been developed and widely used in material and biomedical fields such as quantum dots (QDs) [1], colloidal gold nanoparticles [2], and magnetite (Fe_3O_4) nanoparticles [3] owing to their unique characteristics of large specific surface area, homogeneous size, higher sensitivity, and better function [4, 5]. Among them, fluorescent dye-doped nanoparticles have attracted special attention for several reasons. Firstly, they can provide high intensity of the fluorescent signal for the measurement. The traditional label method could have only one or a few fluorophores to signal one bimolecular recognition event. Fortunately, the dye-doped nanoparticles might contain hundreds to thousands of dye molecules, therefore, an intense fluorescence signal that is up to 30,000 fold better than that of a single organic fluorophore [6–8]. This extreme brightness makes them especially suitable for ultrasensitive bioanalysis and negates the need for additional reagents or signal amplification steps [9]. Secondly, the dye-doped fluorophore could have favorable photostability due to the exclusion of oxygen by matrix encapsulation. Other advantages are the good potential for surface modification with various biomolecules, and easy manufacturing process [6]. These advantages indicated that dye molecules encapsulated in the nanoparticles had high stability and retained their optical activity, thus providing a viable route for various applications with unique properties, such as biochemical and bio-analytical applications [10–13].

However, the biocompatibility of currently available fluorescent nanoparticles is not acceptable, thus limiting their applications *in vivo* [12]. One approach to develop fluorescent nanoparticles with excellent biocompatibility and easy combination with biomacromolecules are to load fluorescent dye into a suitable natural biopolymer carrier [4]. The natural biopolymer gelatin has the characteristics of excellent biocompatibility, nontoxic biodegradation *in vivo*, and readily excreted products. It also has the highly effective drug encapsulation and can be fabricated into various forms of carriers for controlled drug delivery [14]. Nevertheless, because gelatin nanoparticles consist of cross-linkage of peptide side chains, small pores or gaps exist

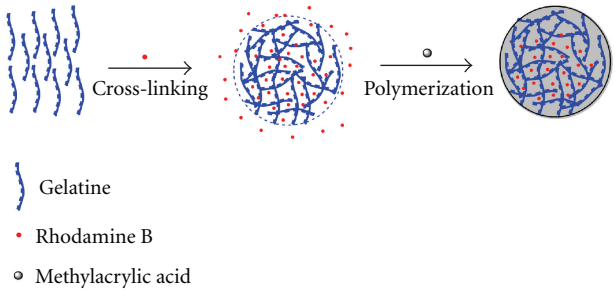

Figure 1: Schematic illustration of preparation for the FPMAAG nanoparticles. Rhodamine B was mixed with gelatin to form gelatin nanoparticles by coacervation and cross-liking. Methylacrylic acid was also mixed before the cross-liking. Next, the temperature of this system was raised to initiate the polymerization. The PMAA combined into the gelatin matrix and formed a coating on the surface of gelatin nanoparticles.

on the nanoparticles surface, which leads to the leakage of encapsulated materials and instability especially for water-soluble dyes or drugs [12, 13]. These limited the application for the fluorescent gelatin nanoparticles.

To overcome this problem, we design a new method for fabricating rhodamine B encapsulated fluorescent poly(methacrylic acid) coated gelatin (FPMAAG) nanoparticles. The strategy of the preparation is to mix the methacrylic acid into the gelatin solution first. After the gelatin nanoparticles were formed through the coacervation method using sodium sulfate as the coacervation reagent and are cross-linked by formaldehyde, the methacrylic acid polymerized slowly under a mild condition by the initiator. This process can lead to the formation of a coating on the surface of the gelatin nanoparticles, as illustrated in Figure 1, which will then block the small pores or gaps. The obtained FPMAAG nanoparticles show a uniform spherical shape, retardant dye releasing, and excellent absorption and fluorescence properties. The fluorescence intensity showed linearity about three orders of magnitude. The FPMAAG nanoparticles were also tested for cell imaging which showed stronger intensity for cell fluorescence imaging and prolonged dye preservation time.

2. Experimental Section

2.1. Chemicals and Materials. Gelatin (Type B, 238–282 Bloom, isoelectric point 4.0–5.7) was purchased from Amresco Inc. (Solon, Ohio, USA). Tween-20 was obtained from Sigma-Aldrich Corporation (St. Louis, Mo. USA). Methacrylic acid was purchased from Tianjin Kermel Chemical Reagents Development Center (Tianjin, China). 2,2′-Azobis 2-methylpropionamide dihydrochloride (AIBA) was purchased from Qingdao Runxing Photoelectric Material Co. Ltd. (Qingdao, China). Rhodamine B was obtained from Sanland Chemical (Los Angeles, USA). Pancreatic cancer cell line PC-2 was purchased from Lab Animal Center, Fourth Military Medical University of China (Xi'an, China). Sodium sulfate, sodium hydroxide, isopropanol, and formaldehyde (37%) were analytical grade and used as purchased. A 14 KD dialyzer was purchased from Sino-American Biotechnology Company. All the chemicals and solvents were used without further purification. Double-distilled water was used in entire process.

2.2. Preparation of FPMAAG Nanoparticles. The preparation method for FPMAAG nanoparticles involved the process of coacervation with sodium sulfate, followed by phase separation using isopropanol, cross-linking by formaldehyde, and initiated polymerization by AIBA. Briefly, FPMAAG nanoparticles were obtained as follows: 10 mL distilled water containing 5 mg rhodamine B, 500 mg sodium hydroxide, and 250 mg gelatin was under continuous stirring for 10 min (300 rpm) at 50°C with a dropwise addition of 500 μL methacrylic acid. After 100 μL of Tween-20 were added as surfactant and the solution was stirred for 5 min, 20% w/w sodium sulfate solution was added dropwise to the mixture until a small amount of precipitation formed, which could be observed as the solution changed from clean to opaque. This was followed by the addition of 400 μL isopropanol for phase separation, which could lead the solution translucent. Next, 4.0 mL formaldehyde was introduced to the mixture as a cross-linking reagent. After stirring for 30 min, 50 mg AIBA was added as an initiator, and the temperature of the system was raised to 60°C. The mixture was maintained at this temperature for 6 hours with continuous stirring to produce rhodamine B encapsulated FPMAAG nanoparticles. The dark-red final product was dialyzed with double-distilled water for 3 days to remove the free rhodamine B and other unreacted reagents. The obtained FPMAAG nanoparticles were filtered through a 200 nm filtration membrane under vacuum and stored at 4°C prior to use.

2.3. Morphology Analysis and Spectra Properties. The morphology of FPMAAG nanoparticles was evaluated through transmission electron microscopy (TEM, JEM-2100F, JOEL, Japan) observations. Size distribution of the FPMAAG nanoparticles was determined using dynamic light scattering (DLS, Malvern Zetasizer Nano ZS90, Malvern instruments Ltd., UK).

Functional groups on the surface of the FPMAAG nanoparticles were evaluated by a Fourier transform infrared spectrometer (FTIR, IR presitge-21, Japan). In a typical procedure, 5 mL of dialyzed FPMAAG nanoparticles solution was lyophilized to powder. These powder were mixed with IR-grade KBr (0.1 g), pressed into tablet form, and then the spectrum recorded. Pure gelatin and MAA were also measured for comparison.

Fluorescent spectra were measured by FluoroMax-4 (Horiba Jobin Yvon, NJ, USA) with excitation and emission slits both set to 2 nm. UV-Vis absorption spectra were measured by T-6 UV-Vis spectrophotometers (Purkinje general, Beijing, China) using double-distilled water as blank. The loading efficiency of rhodamine B was the amount of encapsulated rhodamine B in the FPMAAG nanoparticles, which was determined by UV-Vis and fluorescence measurements using a series of standard rhodamine B solutions as calibration.

The retardant release of the FPMAAG nanoparticles was assessed by dynamic dialysis method as reported [14]. Briefly,

the newly prepared FPMAAG nanoparticles mixture solution containing 5.0 mg rhodamine B was placed into a dialysis bag and placed in 1000 mL of double-distilled water with magnetic stirring at 200 rpm and 25°C. At predetermined time intervals, 1.5 mL of release medium was withdrawn, and the rhodamine B content was determined by UV-Vis absorption spectra at wavelength of 555 nm. The gelatin nanoparticles without PMAA coating and the PMAA system without the addition of gelatin were also measured for comparisons.

To examine the quantitative potential of the FPMAAG nanoparticles, serial dilution of FPMAAG solutions was prepared with various concentrations of encapsulated rhodamine B which covered three orders of magnitude, from 4.0 ng·mL^{-1} to 4.0 μg·mL^{-1}. Fluorescent spectra measurements of these solutions was carried out under the same condition as mentioned above. The peak fluorescence intensities were plotted against the concentration of encapsulated rhodamine B to show as a calibration curve. Linear range and linearity of the calibration curve were discussed.

2.4. Fluorescence Imaging of Cells. Pancreatic cancer cell line PC-2 were incubated in 100 mL growth buffer as adherent cells according to the manufacturer's instructions and at 37°C in an atmosphere containing 50 mL·L^{-1} CO_2 and 950 mL·L^{-1} with a relative humidity until labeling. Then the cells were incubated for 15 min at room temperature, washed 3 times with cold PBS (137 mmol·L^{-1} NaCl, 2.7 mmol·L^{-1} KCl, 10 mmol·L^{-1} Na_2HPO_4, 1.8 mmol·L^{-1} KH_2PO_4, pH 7.4), and incubated with the FPMAAG nanoparticles (10.0 mg·mL^{-1} in 5.0 mL buffer solution) for 45 min at room temperature. To demonstrate the cells label results of FPMAAG nanoparticles, fluorescence images of the cells were observed by fluorescence microscope (Olympus CX41, Japan) excited by 520 nm laser (Olympus U-RFLT50, Japan) at room temperature. The direct incubation of rhodamine B and cells were carried out as controls.

3. Results and Discussions

3.1. Preparation and Morphology of FPMAAG Nanoparticles. In the preparation process, methacrylic acid was chosen because it could form a polymeric layer to retard the release of encapsulated drug in a hydrogel drug delivery system [15]. Vishal Gupta et al. reported that by adding a PMAA system to the gelatin polymers, the formation of a Gelatin-PMAA interpenetrating polymer hydrogel system could retard the drug release at an acidic pH [16]. In our study, the FPMAAG nanoparticles were prepared by coacervation and phase separation method, the PMAA could form a protection layer at the surface of gelatin nanoparticles. The preparation was carried out at an alkaline pH, which was required by the cross-linking reaction of gelatin nanoparticles using formaldehyde as the cross-linking reagent. Consequently, after dialysis to remove the free rhodamine B and other unreacted reagents, and using under physiological conditions, the surrounding solution of the FPMAAG nanoparticles was changed to a neutral pH which could retard the release of encapsulated rhodamine B from the nanoparticles. The other advantage of adding methacrylic acid to the gelatin mixture was the increased solubility of gelatin at the preparation step, which can reduce preparation time and results in a narrow range of size distribution of the FPMAAG nanoparticles.

For the preparation of Gelatin-PMAA nanoparticles, a higher reaction temperature was used in this study compared to the previous research of our group [17]. Jahanshahi et al. discussed that at low temperature, gelatin nanoparticles are not easy to form because gelatin is in a highly viscous gel formation at that condition. At a temperature above 50°C, the gelatin chain could uncoil sufficiently to be in a better condition for nanoparticles formation [18]. Meanwhile, a higher temperature could reduce the time for the cross-linking of gelatin to form nanoparticles and for the polymerization of the PMAA coating layer. On the other hand, if the reaction temperature is too high, the organic dye encapsulated in the nanoparticles could be decomposed due to some side reactions. Given all these concerns, the reaction temperature in the present study was thus set to 50°C at the mixture step and raised to 60°C for the polymerization. Under this condition, the polymerization could be initiated by the AIBA, and the formation of PMAA will be completed in 6 hours.

In the preparation process of FPMAAG nanoparticles, formaldehyde was used as a cross-linking reagent rather than glutaraldehyde which was usually used in reported papers [17, 19], because glutaraldehyde could form a dark-yellow solution with amino acid when the temperature was above 50°C. This colored solution could interfere with the absorption and fluorescence measurement of FPMAAG nanoparticles. Formaldehyde is known to react with several peptide side chain groups, especially lysine residues along the gelatin chain in order to form a methylene bridge or a cross-linkage [20]. With this cross-linking reaction, the final FPMAAG nanoparticle product could remain transparent, which could avoid the effect of the yellow-colored byproduct of glutaraldehyde on the absorption and fluorescence characteristics of the encapsulated rhodamine B. The optimized pH range for the cross-linking of formaldehyde is 8-9. Thus, the acidity of the reaction should be carefully adjusted in the mixing step with enough sodium hydroxide to neutralize the added methacrylic acid.

The morphology and size distribution of the FPMAAG nanoparticles was examined by TEM (Figure 2) and size analyzer (Figure 3). The FPMAAG nanoparticles were spherically shaped with a diameter of approximately 60 ± 5 nm, which was consistent with the results from the previous study of our group (46 nm) [17]. The increased size could attribute to the formation of PMAA coating layer. From Figure 2, the dark core of gelatin nanoparticles with gray shell of PMAA coating were also observed. From literature searching, the available reported preparation methods for gelatin hydrogels were in the formation of a piece of sheet with a thickness in the scale of millimeters [16], or a nanosphere with a diameter around the micrometers scale [21]. For the preparation of gelatin particles in nanometer scales, Gupta et al. prepared a series of gelatin nanoparticles measuring 37 nm by the reverse micelle method [22]. Another commonly used method was the addition of acetone to the gelatin aqueous

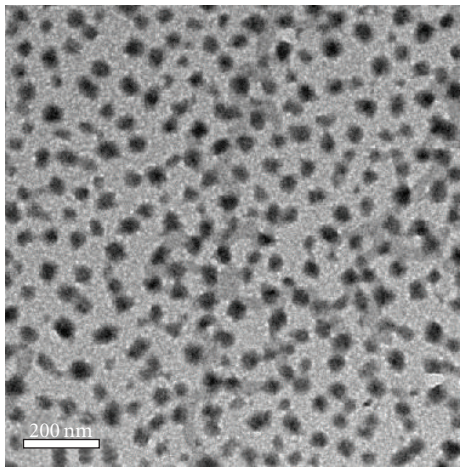

Figure 2: TEM image of PMAA coated gelatin nanoparticles.

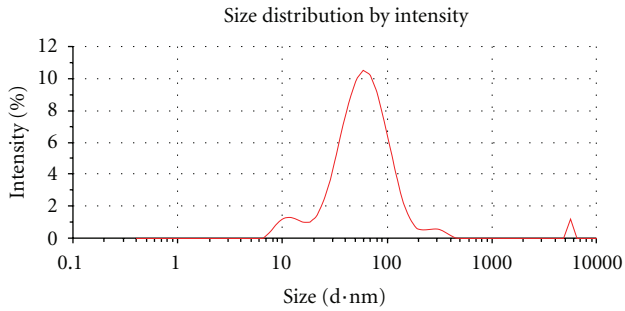

Figure 3: Size distribution of FPMAAG nanoparticles.

solution to form the precipitation of gelatin nanoparticles with a diameter of about 50 nm [18, 21]. In our coacervation method, the diameters of the gelatin nanoparticles were controlled around 60 nm by the gelatin concentration and the amount of added inorganic coacervation reagent. With higher gelatin concentration and more sodium sulfate added, the diameter of the nanoparticles will increase. On the other hand, if a lower stirring velocity was used, it would cause the increase of nanoparticles diameter. Meanwhile, a higher temperature or longer reaction time for the cross-linking would also increase the nanoparticles diameter. With many attempts, the optical conditions for the preparation of FPMAAG nanoparticles were determined as mentioned in the experimental section. In addition, there was no hydrophobic solvent used to avoid the washing step concerning the biochemical applications.

3.2. IR Spectra of FPMAAG Nanoparticles. Figure 4 shows the IR spectra of the FPMAAG nanoparticles powder prepared by lyophilizing the dialyzed PMAAG nanoparticles blank solution which had not encapsulated any rhodamine B. To make a clear comparison, the IR spectra of gelatin and methacrylic acid were also presented in the same figure. The transparencies of the three spectra were normalized and separated for the convenience of comparison, so the Y-axis was set in arbitrary unit (a.u.). From the IR spectra, the moderate stretching vibration of the N–H bond can be observed around 3300 nm^{-1} which revealed the existence of amide in the gelatin compared to the IR spectra of gelatin [23]. The strong absorption at 2900 nm^{-1} is due to the stretching vibration of the C-H bond in the PMAA coating of the FPMAAG nanoparticles. Strong absorption at 1650 nm^{-1} is the evidence that carbonyl group exists in the FPMAAG nanoparticles, which were derived from the carboxyl group of methacrylic acid. From the attribution of IR peaks of FPMAAG nanoparticles between 1000 and 1500 nm^{-1} to the IR spectra of either gelatin or methacrylic acid, a conclusion regarding the formation of PMAA combining into gelatin matrix could be drawn.

3.3. Absorption Spectra of FPMAAG Nanoparticles. UV-Vis absorption and fluorescence emission spectra of the FPMAAG nanoparticles solution are shown in Figure 5. The fluorescence spectrum was normalized to the same level of absorption spectrum in the same figure for a clear comparison. The absorption and normalized fluorescence emission spectra of rhodamine B aqueous solution (0.8 $\mu g \cdot mL^{-1}$) are also shown in the same figure. The absorption and emission peak of encapsulated rhodamine B was found to have no significant change compared to the rhodamine B dissolved in water with an absorption peak at 555 nm and an emission peak at 575 nm, which were mirror images of each other. This result meant that the formed FPMAAG nanoparticles are transparent and have no effect on the optical behavior of the encapsulated organic dye.

From the absorbance of UV-Vis spectra, the total amount of encapsulated rhodamine B in the FPMAAG nanoparticles could be calculated as 82 ± 5 μg after three days of dialysis. It was assumed that the molar extinction coefficient (ε) of encapsulated rhodamine B had no change compared with the rhodamine B dissolved in distilled water. Thus, a series of rhodamine B aqueous solution with different concentrations were used as calibration. On the other hand, a certain volume of FPMAAG nanoparticles solution was lyophilized, and the powder was weighed. The total mass of the FPMAAG nanoparticles was 310 mg. Thus, the rhodamine B loading efficiency of the FPMAAG nanoparticles was 0.26 μg per mg nanoparticles.

3.4. Fluorescence Spectra of FPMAAG Nanoparticles. Based on the fluorescence intensity of fluorescent emission in Figure 5, we also calculated that the amount of encapsulated rhodamine B in the FPMAAG nanoparticles was 65 ± 5 μg after three days of dialysis. This was consistent with the amount calculated by UV-Vis absorption measurement. The pH effect on the fluorescence intensity of FPMAAG nanoparticles was carried out by dilute same amounts of FPMAAG nanoparticles solution to the same volume with different PBS buffer (pH = 6.0, 7.0, 8.0, and 9.0, resp.). The fluorescence intensities of these serial solutions had no significant differences (data not shown). The same amount of FPMAAG nanoparticles were also diluted with different KCl solution (concentration of KCl were 0.01, 0.02, 0.05, 0.1, and 0.2 M, resp.) to verify the effect of ionic strength to the fluorescence intensity. The fluorescence intensities kept at the same level with various ionic strengths (data not shown).

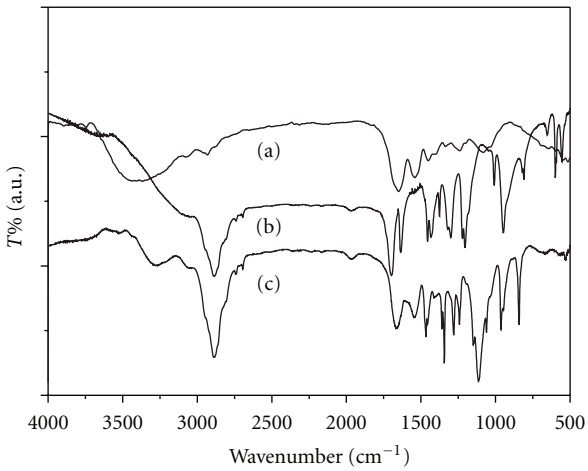

(a) Gelatin

(b) MAA

(c) PMAA coated gelatin nanoparticles

Figure 4: IR spectra of gelatin (a), methacrylic acid (b), and PMAA coated gelatin nanoparticles (c). The transparences of the three spectra were normalized and separated for the convenience of comparison.

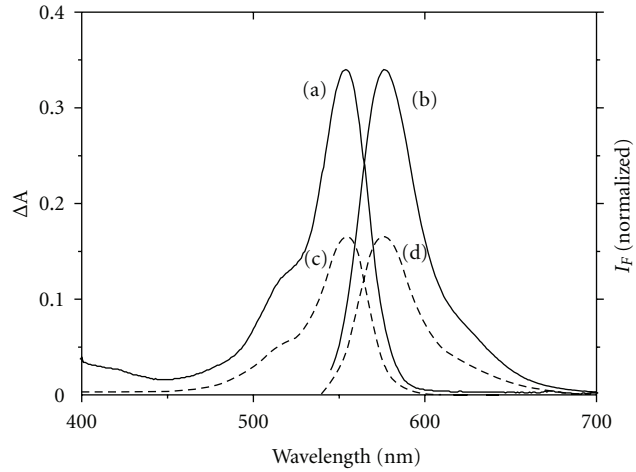

Figure 5: Absorption (a) and fluorescence (b) spectra of FPMAAG nanoparticles compared with absorption (c) and fluorescence (d) spectra of rhodamine B aqueous solution ($0.8\,\mu g\cdot mL^{-1}$). The intensity of fluorescence spectra were normalized to make a clear comparison.

These results revealed that the encapsulated rhodamine B in the FPMAAG nanoparticles still had strong emission intensity and high fluorescent yield, which means that the nanoparticles were transparent for the encapsulated dye to perform its optical behavior. Meanwhile, the nanoparticles could provide a suitable environment for the dye molecules to be concentrated at a certain location with high emission efficiency. The protection and concentration of rhodamine B provided by the nanoparticles could result in enhanced emission intensity with lower dye concentration compared to the rhodamine B solution, which could be used for higher sensitive fluorescence tracing in the future.

3.5. Fluorescence Calibration Curve Fitting. To evaluate the possibility for quantitative bioanalytical applications, linear relationships between concentrations of FPMAAG nanoparticles and fluorescence emission intensity were examined. From the fluorescence intensities of series diluted FPMAAG nanoparticles solutions, a linear curve fitting was obtained as shown in Figure 6. The linear relationships between fluorescence intensity and concentration of encapsulated rhodamine B in FPMAAG nanoparticles were confirmed ranging from $4.0\,ng\cdot mL^{-1}$ to $0.4\,\mu g\cdot mL^{-1}$ with the linear regression equations: $I_F = 1.29 \times 10^7 C + 5.68 \times 10^4$ and correlation coefficient $R^2 = 0.9990$, where I_F and C referred to fluorescence intensity and concentration of rhodamine B encapsulated in FPMAAG nanoparticles, respectively. The fluorescence intensities obtained at the concentration from 0.8–$4.0\,\mu g\cdot mL^{-1}$ were not in the linear relationship because the fluorescence emissions were too strong which were out of the signal response range of the fluorescence spectrometer. By these attempts, the wide linear range that covers three orders of magnitude could be confirmed. The rhodamine B-doped silica nanoparticles for the quantitative determination of aflatoxin B_1 using competitive-type fluorescence immunoassay by Tang et al. have been reported recently [9]. The linear response range was only one order of magnitude (0.5–$7\,ng\cdot mL^{-1}$ for aflatoxin B_1). Another research using rhodamine B adsorbed golden nanoparticles for the quantitative detection of mercury had a linear correlation the range of 15–250 nM [24]. By the comparison of our FPMAAG nanoparticles system with the reported dye-doped nanoparticles, a more accurate and sensitive fluorescence bioanalytical method could be established in the future.

3.6. Retardant Release of Rhodamine B. To study the retardant release of the FPMAAG nanoparticles, the dynamic dialysis was carried out for the measurement of release of encapsulated rhodamine B. The results were shown in Figure 7. After the beginning of the dynamic dialysis, the rhodamine B contents in the release medium were increased dramatically within 30 hours for all three solutions. After that, the release of rhodamine B in FPMAAG nanoparticles was slowed and saturated after 60 hours with a release percentage of 60%. As comparison, the release profile of PMAA solution in the absence of gelatin showed a free release of rhodamine B, which indicated that only the polymerization of MAA could not hold rhodamine B. The sample of gelatin nanopartilces without PMAA coating showed a faster release of encapsulated rhodamine B with a release percentage around 80% after 60 hours dialysis. The fast release at the beginning of dynamic dialysis experiment for FPMAAG nanoparticles could be due to the release of the free rhodamine B in the mixture. After 40 hours dialysis, the increased rhodamine B content in the release medium was contributed to the release of encapsulated rhodamine B, which showed a retardant release property compared to the gelatin nanoparticles without PMAA coating.

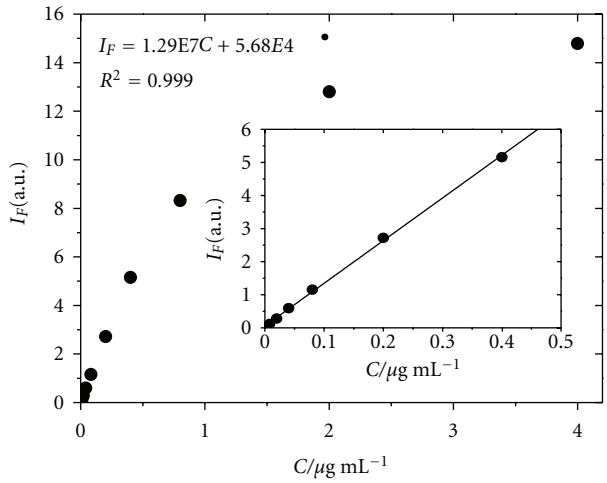

Figure 6: Calibration curve of FPMAAG nanoparticles solution. The concentration of encapsulated rhodamine B ranged from 4.0 ng·mL^{-1} to 4.0 μg·mL^{-1}. Insert was the linear curve fitting from 4.0 ng·mL^{-1} to 0.4 μg·mL^{-1}.

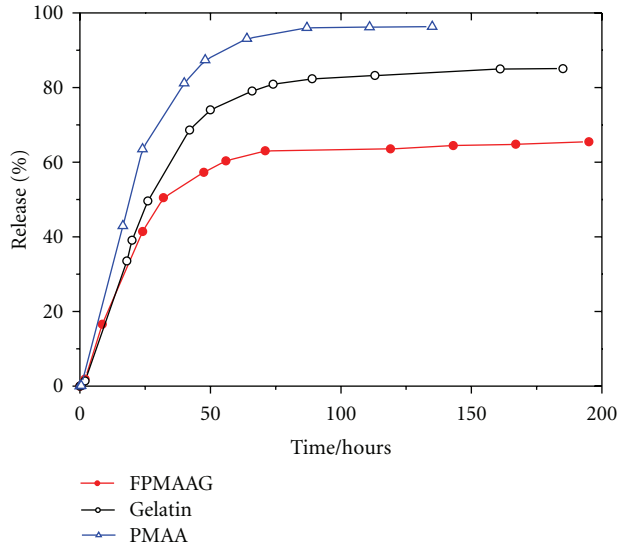

Figure 7: Dynamic dialysis release curve of FPMAAG nanoparticles (solid circle), gelatin nanoparticles without PMAA coating (opened circle), and PMAA system in the absence of gelatin (opened triangle). Double-distilled water was used as dialysis medium.

We continued the dialysis after the saturated rhodamine B content was reached. The pink color of the PFMAAG nanoparticles solution did not vanish until after two weeks had passed. As comparison, the pink the rhodamine B encapsulated gelatin nanoparticles without PMAA coating disappeared within 3 days. It was reported that the release of encapsulated medicine in gelatin nanoparticles would be completed in 100 hours [14, 22, 25–28], while our FPMAAG nanoparticles could be maintained at a certain concentration after six days of dialysis. The retardant dye release property indicates that PMAA, which combined into the gelatin matrix and formed a coating layer on the

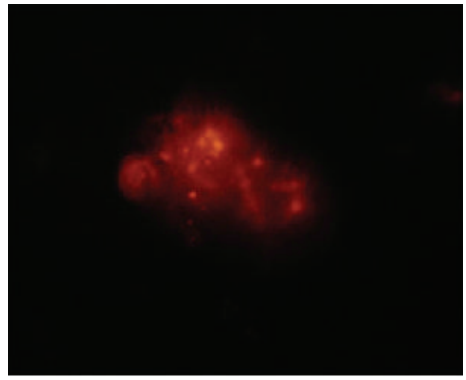

Figure 8: Fluorescence imaging of pancreatic cancer cell line PC-2 incubated with FPMAAG nanoparticles. Excitation wavelength was set at 520 nm.

gelatin nanoparticles, had a protective effect because it can block the pores on the surface of gelatin nanoparticles and thus delay the release of encapsulated rhodamine B. One of the reasons for the retardance could be the methyl groups of the methacrylic acid, which could form a branch structure after polymerization to block the release of rhodamine B encapsulated in the gelatin nanoparticles. Another reason could be the combination of PMAA into gelatin matrix that results in a transfer barrier between the interfaces to retard the release of rhodamine B. Obtaining a more detailed mechanism and investigating the controlled release of FPMAAG nanoparticles will be our next goal. The elongated release time of the FPMAAG nanoparticles could be used for biochemical and bioanalytical applications in the future.

3.7. Fluorescence Imaging of Cells. The fluorescence imaging of pancreatic cancer cell line PC-2 was shown in Figure 8. After 45 min of incubation, the fluorescence imaging of pancreatic cancer cells were observed. It suggested that FPMAAG nanoparticles could penetrate the membrane of cell and be endocytosed easily. This property of FPMAAG nanoparticles was resulted from the small size of the nanoparticles. It was also derived from the excellent biocompatibility of gelatin and PMAA, which made the nanoparticles could not be rejected by the cells.

From the fluorescence imaging, the FPMAAG nanoparticles could be observed with strong red emission, which were the aggregation of nanoparticles. The FPMAAG nanoparticles didn't distribute uniformly in the cell that could be attributed to the different affinity of the organelle to the FPMAAG nanoparticles. Additionally, the strong emission under the fluorescence microscope could sustain for 15 hours compared with 3 hours for the direct incubation of rhodamine B and cells. The easy endocytosis and sustained retention time suggested that FPMAAG nanoparticles were an excellent candidate for cell imaging and targeting [29–32]. After cross-liking with ligand, the FPMAAG could be used as promising a targeting and therapy label for specific receptor in cells in our future research.

4. Conclusions

In summary, rhodamine B encapsulated PMAA coated gelatin nanoparticles were prepared using an improved coacervation and phase separation method with formaldehyde as a cross-linking reagent at 60°C. The polymerization of methacrylic acid was initiated after the cross-linking. IR spectra confirmed that poly(methacrylic acid) combining into gelatin matrix which could block the pores of gelatin nanoparticles. From TEM image, the diameter of FPMAAG nanoparticles was measured. The coating of PMAA layer on the surface of gelatin nanoparticles was also confirmed. The UV-Vis and fluorescence measurements showed that the encapsulated rhodamine B could have excellent spectral properties. The FPMAAG nanoparticles were stable and the encapsulated rhodamine B was released at a slower rate compared with the rates of gelatin nanoparticles without PMAA coating. The linear relationships between fluorescence intensity and nanoparticles concentration were over three orders of magnitude. In the fluorescence imaging of pancreatic cancer cell line PC-2, the FPMAAG nanoparticles also showed excellent biocompatibility and sustained retention time. The results indicate a high fluorescent yield of the FPMAAG nanoparticles thus; it could provide a promising functional nanoparticles material for biochemical and bioanalytical applications.

Acknowledgment

This study was supported in part by National Basic Research Program 973 of China (No. 2010CB732603), and National Nature Science Foundation of China (Nos. 30772658, 20905060, and 30970712).

References

[1] I. L. Medintz, H. T. Uyeda, E. R. Goldman, and H. Mattoussi, "Quantum dot bioconjugates for imaging, labelling and sensing," *Nature Materials*, vol. 4, no. 6, pp. 435–446, 2005.

[2] M. C. Daniel and D. Astruc, "Gold nanoparticles: assembly, supramolecular chemistry, quantum-size-related properties, and applications toward biology, catalysis, and nanotechnology," *Chemical Reviews*, vol. 104, no. 1, pp. 293–346, 2004.

[3] Y. W. Jun, J. W. Seo, and J. Cheon, "Nanoscaling laws of magnetic nanoparticles and their applicabilities in biomedical sciences," *Accounts of Chemical Research*, vol. 41, no. 2, pp. 179–189, 2008.

[4] S. Sushmitha, K. Joydip, and C. K. Subhas, "Biopolymeric nanoparticles," *Science and Technology of Advanced Materials*, vol. 11, no. 1, article 014104, 2010.

[5] J. Kim, Y. Piao, and T. Hyeon, "Multifunctional nanostructured materials for multimodal imaging, and simultaneous imaging and therapy," *Chemical Society Reviews*, vol. 38, no. 2, pp. 372–390, 2009.

[6] L. Wang, K. Wang, S. Santra et al., "Watching silica nanoparticles glow in the biological world," *Analytical Chemistry*, vol. 78, no. 3, pp. 646–654, 2006.

[7] W. Lian, S. A. Litherland, H. Badrane et al., "Ultrasensitive detection of biomolecules with fluorescent dye-doped nanoparticles," *Analytical Biochemistry*, vol. 334, no. 1, pp. 135–144, 2004.

[8] M. Nakamura, M. Shono, and K. Ishimura, "Synthesis, characterization, and biological applications of multifluorescent silica nanoparticles," *Analytical Chemistry*, vol. 79, no. 17, pp. 6507–6514, 2007.

[9] D. Tang, Y. Yu, R. Niessner, M. Miró, and D. Knopp, "Magnetic bead-based fluorescence immunoassay for aflatoxin B1 in food using biofunctionalized rhodamine B-doped silica nanoparticles," *Analyst*, vol. 135, no. 10, pp. 2661–2667, 2010.

[10] W. Yang, C. G. Zhang, H. Y. Qu, H. H. Yang, and J. G. Xu, "Novel fluorescent silica nanoparticle probe for ultrasensitive immunoassays," *Analytica Chimica Acta*, vol. 503, no. 2, pp. 163–169, 2004.

[11] Z. Tian, W. Wu, and A. D. Q. Li, "Photoswitchable fluorescent nanoparticles: preparation, properties and applications," *ChemPhysChem*, vol. 10, no. 15, pp. 2577–2591, 2009.

[12] F. Wang, W. B. Tan, Y. Zhang, X. Fan, and M. Wang, "Luminescent nanomaterials for biological labelling," *Nanotechnology*, vol. 17, no. 1, pp. R1–R13, 2006.

[13] A. Burns, H. Ow, and U. Wiesner, "Fluorescent core-shell silica nanoparticles: towards "lab on a particle" architectures for nanobiotechnology," *Chemical Society Reviews*, vol. 35, no. 11, pp. 1028–1042, 2006.

[14] G. K. Saraogi, P. Gupta, U. D. Gupta, N. K. Jain, and G. P. Agrawal, "Gelatin nanocarriers as potential vectors for effective management of tuberculosis," *International Journal of Pharmaceutics*, vol. 385, no. 1-2, pp. 143–149, 2010.

[15] N. Zhang and W. Knoll, "Thermally responsive hydrogel films studied by surface plasmon diffraction," *Analytical Chemistry*, vol. 81, no. 7, pp. 2611–2617, 2009.

[16] N. Vishal Gupta, C. S. Satish, and H. G. Shivakumar, "Preparation and characterization of gelatin-poly(methacrylic acid) interpenetrating polymeric network hydrogels as a pH-sensitive delivery system for glipizide," *Indian Journal of Pharmaceutical Sciences*, vol. 69, no. 1, pp. 64–68, 2007.

[17] D. Wu and M. Wan, "A novel fluoride anion modified gelatin nanogel system for ultrasound-triggered drug release," *Journal of Pharmacy & Pharmaceutical Sciences*, vol. 11, no. 4, pp. 32–45, 2008.

[18] M. Jahanshahi, M. H. Sanati, S. Hajizadeh, and Z. Babaei, "Gelatin nanoparticle fabrication and optimization of the particle size," *Physica Status Solidi A*, vol. 205, no. 12, pp. 2898–2902, 2008.

[19] Z. Lu, T. K. Yeh, M. Tsai, J. L. S. Au, and M. G. Wientjes, "Paclitaxel-loaded gelatin nanoparticles for intravesical bladder cancer therapy," *Clinical Cancer Research*, vol. 10, no. 22, pp. 7677–7684, 2004.

[20] M. Madaghiele, A. Piccinno, M. Saponaro, A. Maffezzoli, and A. Sannino, "Collagen- and gelatine-based films sealing vascular prostheses: evaluation of the degree of crosslinking for optimal blood impermeability," *Journal of Materials Science: Materials in Medicine*, vol. 20, no. 10, pp. 1979–1989, 2009.

[21] C. J. Coester, K. Langer, H. Von Briesen, and J. Kreuter, "Gelatin nanoparticles by two step desolvation—a new preparation method, surface modifications and cell uptake," *Journal of Microencapsulation*, vol. 17, no. 2, pp. 187–193, 2000.

[22] A. K. Gupta, M. Gupta, S. J. Yarwood, and A. S. G. Curtis, "Effect of cellular uptake of gelatin nanoparticles on adhesion, morphology and cytoskeleton organisation of human fibroblasts," *Journal of Controlled Release*, vol. 95, no. 2, pp. 197–207, 2004.

[23] Z. Dong, Q. Wang, and Y. Du, "Alginate/gelatin blend films and their properties for drug controlled release," *Journal of Membrane Science*, vol. 280, no. 1-2, pp. 37–44, 2006.

[24] C. C. Huang and H. T. Chang, "Selective gold-nanoparticle-based "turn-on" fluorescent sensors for detection of mercury(II) in aqueous solution," *Analytical Chemistry*, vol. 78, no. 24, pp. 8332–8338, 2006.

[25] G. Kaul and M. Amiji, "Long-circulating poly(ethylene glycol)-modified gelatin nanoparticles for intracellular delivery," *Pharmaceutical Research*, vol. 19, no. 7, pp. 1061–1067, 2002.

[26] T. G. Shutava, S. S. Balkundi, P. Vangala et al., "Layer-by-layer-coated gelatin nanoparticles as a vehicle for delivery of natural polyphenols," *ACS Nano*, vol. 3, no. 7, pp. 1877–1885, 2009.

[27] M. A. Vandelli, M. Romagnoli, A. Monti et al., "Microwave-treated gelatin microspheres as drug delivery system," *Journal of Controlled Release*, vol. 96, no. 1, pp. 67–84, 2004.

[28] J. Wang, Y. Tabata, and K. Morimoto, "Aminated gelatin microspheres as a nasal delivery system for peptide drugs: evaluation of in vitro release and in vivo insulin absorption in rats," *Journal of Controlled Release*, vol. 113, no. 1, pp. 31–37, 2006.

[29] C. Chotimarkorn, R. Nagasaka, H. Ushio, T. Ohshima, and S. Matsunaga, "Development of novel fluorescent probe 3-perylene diphenylphosphine for determination of lipid hydroperoxide with fluorescent image analysis," *Biochemical and Biophysical Research Communications*, vol. 338, no. 2, pp. 1222–1228, 2005.

[30] D. Varghai, K. Azizuddin, Y. Ahmad, N. L. Oleinick, and D. Dean, "Fluorescence of Pc 4 in U87 cells following photodynamic therapy," in *Photonic Therapeutics and Diagnostics III*, vol. 6424, article 64242A of *Proceedings of SPIE*, San Jose, Calif, USA, January 2007.

[31] E. Q. Song, G. P. Wang, H. Y. Xie et al., "Visual recognition and efficient isolation of apoptotic cells with fluorescent-magnetic-biotargeting multifunctional nanospheres," *Clinical Chemistry*, vol. 53, no. 12, pp. 2177–2185, 2007.

[32] M. Goutayer, S. Dufort, V. Josserand et al., "Tumor targeting of functionalized lipid nanoparticles: assessment by in vivo fluorescence imaging," *European Journal of Pharmaceutics and Biopharmaceutics*, vol. 75, no. 2, pp. 137–147, 2010.